Shen et al., http://www.jcb.org/cgi/content/full/jcb.201204010/DC1

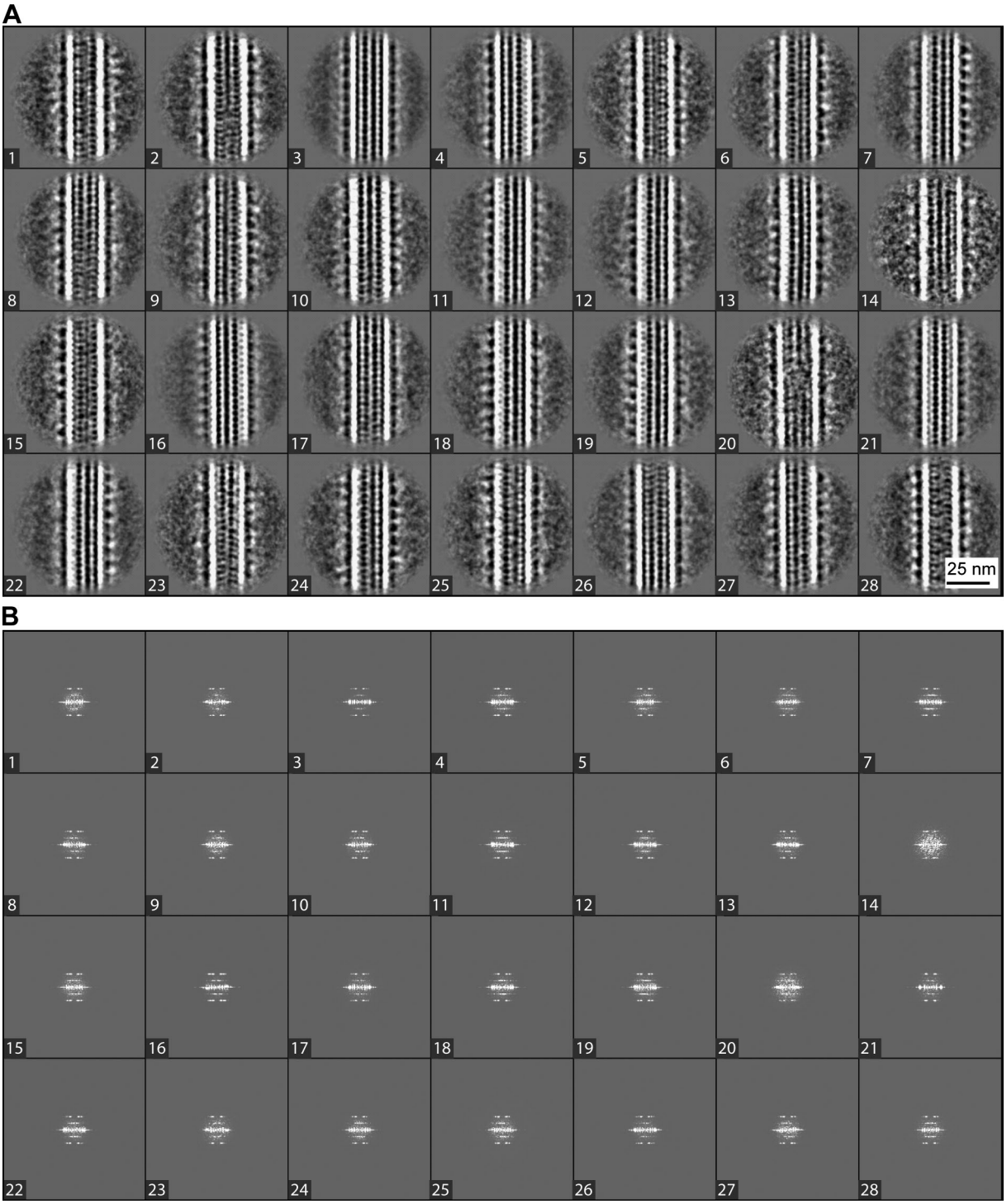

Figure S1. **2D class averages of WHAMM on MTs and respective power spectrums.** (A) 8,186 single images were classified into 28 classes. (B) The respective power spectrums of 28 classes.

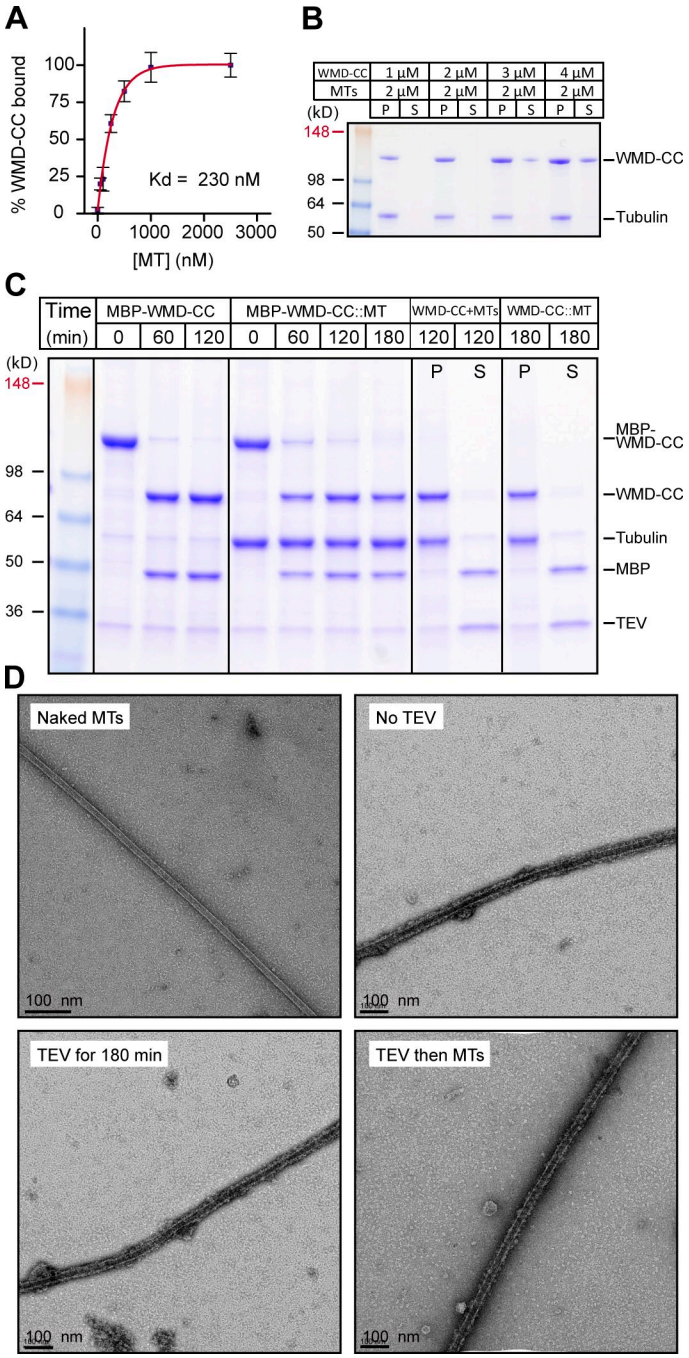

Figure S2. **The MT-binding properties of uncleaved and cleaved versions of MBP-WMD-CC.** (A) Cosedimentation assays were performed using 100 nM MBP-WMD-CC and various concentrations of polymerized tubulin heterodimers. The red line is the fitted curve to the original data points. Error bars show the range of data, which is calculated by subtracting the lowest value from the highest value. (B) Cosedimentation assays were performed using various concentrations of MBP-WMD-CC and 2 μM polymerized tubulin heterodimers. A representative Coomassie blue–stained gel is shown. (C) Free or MT-bound MBP-WMD-CC was treated with the TEV protease for the indicated times and analyzed directly by SDS-PAGE or mixed with MTs (for free MBP-WMD-CC only) and separated into pellet and supernatant fractions before SDS-PAGE analyses. (D) Negatively stained EM images are shown for MBP-WMD-CC and MT complex in different conditions. P, pellet; S, supernatant.

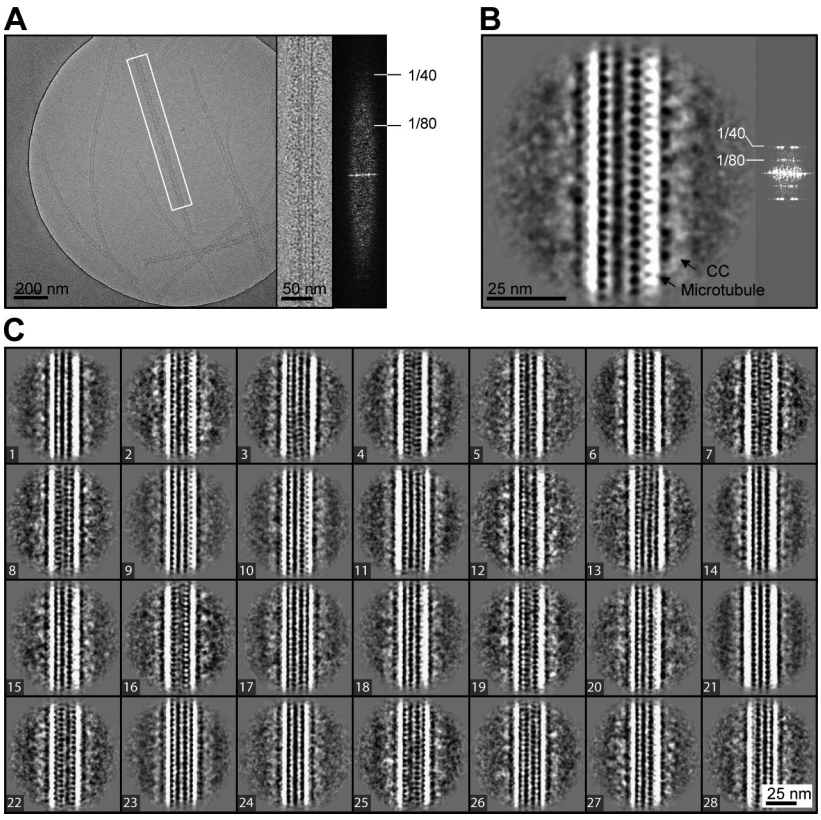

Figure S3. **CC forms helical structures on MTs.** (A) Cryo-EM micrograph of the CC::MT complex and FFT analysis of a selected CC::MT complex filament. The right image shows the existence of 40- and 80-Å^{-1} layer lines. The box is to box filament for FFT analysis, the result of which is shown on the right. (B) One representative class average and its power spectrum. In the power spectrum figures, 40- and 80-Å^{-1} layer lines are marked. (C) 5,030 single images were grouped into 28 classes.

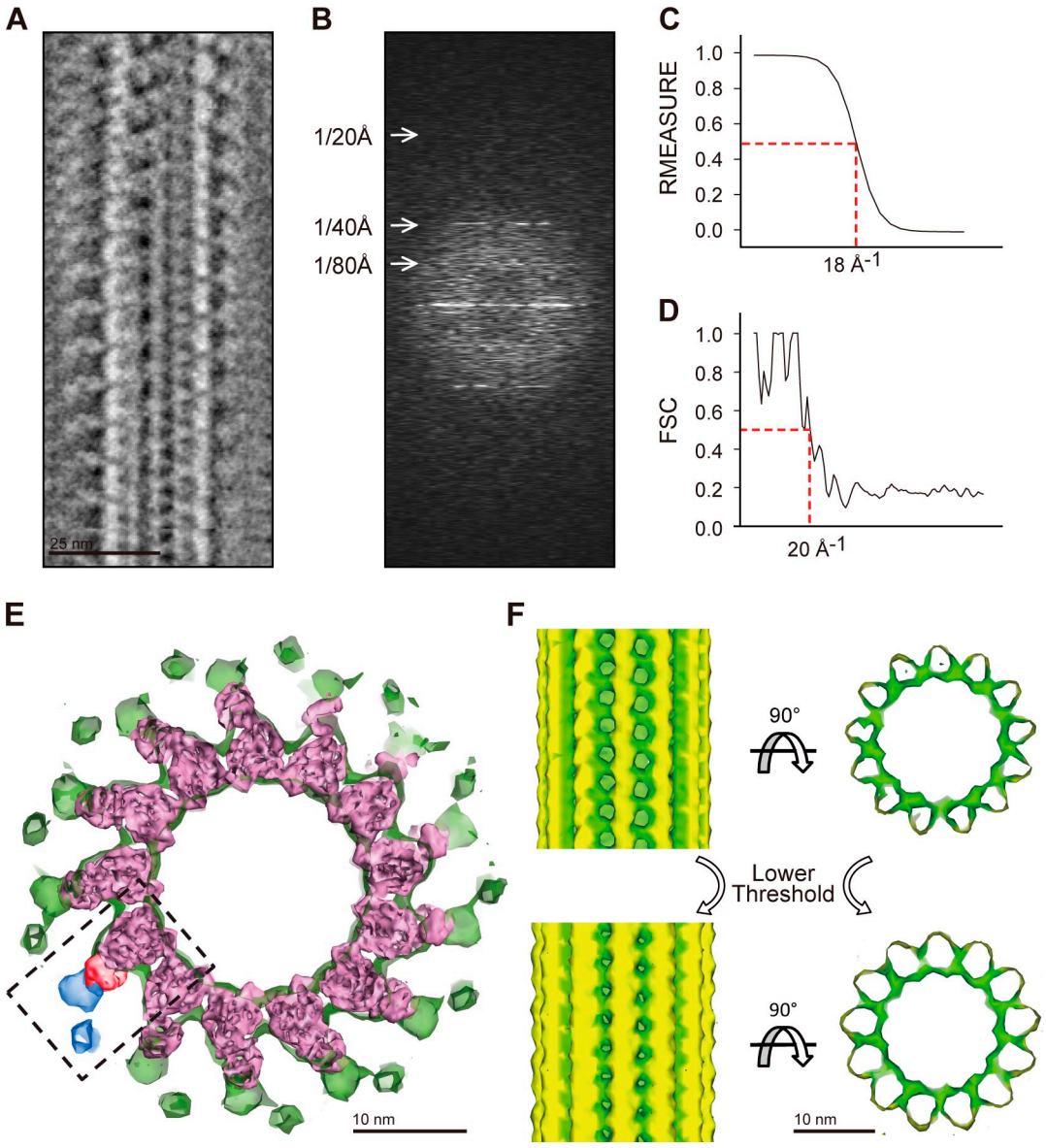

Figure S4. **Resolution estimation and reference unbiased character of WHAMM::MT reconstruction.** (A) Aligned, averaged, and stacked image segments from the WHAMM-decorated MT. (B) Power spectrum of the WHAMM-decorated MT from A. (C) RMEASURE curve of WHAMM::MTs reconstruction. (D) Fourier shell correlation (FSC) curve of WHAMM::MTs reconstruction. The red dotted lines were used to point out the values corresponding to 0.5 in both RMEASURE (C) and Fourier shell correlation (D) methods. (E) Structural comparison of WHAMM::MT and kinesin::MT. WHAMM::MT is colored in green, and kinesin::MT is colored in purple. In the dashed rectangle, the red density is from kinesin and the blue density is obtained from WHAMM. (F) 3D reconstruction of naked MTs using the same reconstruction strategy. Different views of 3D reconstruction of MTs are shown. The threshold is decreased from 0.05 to 0.04 (σ from 2.07 to 1.34) without any appearance of additional densities on the periphery of MTs.

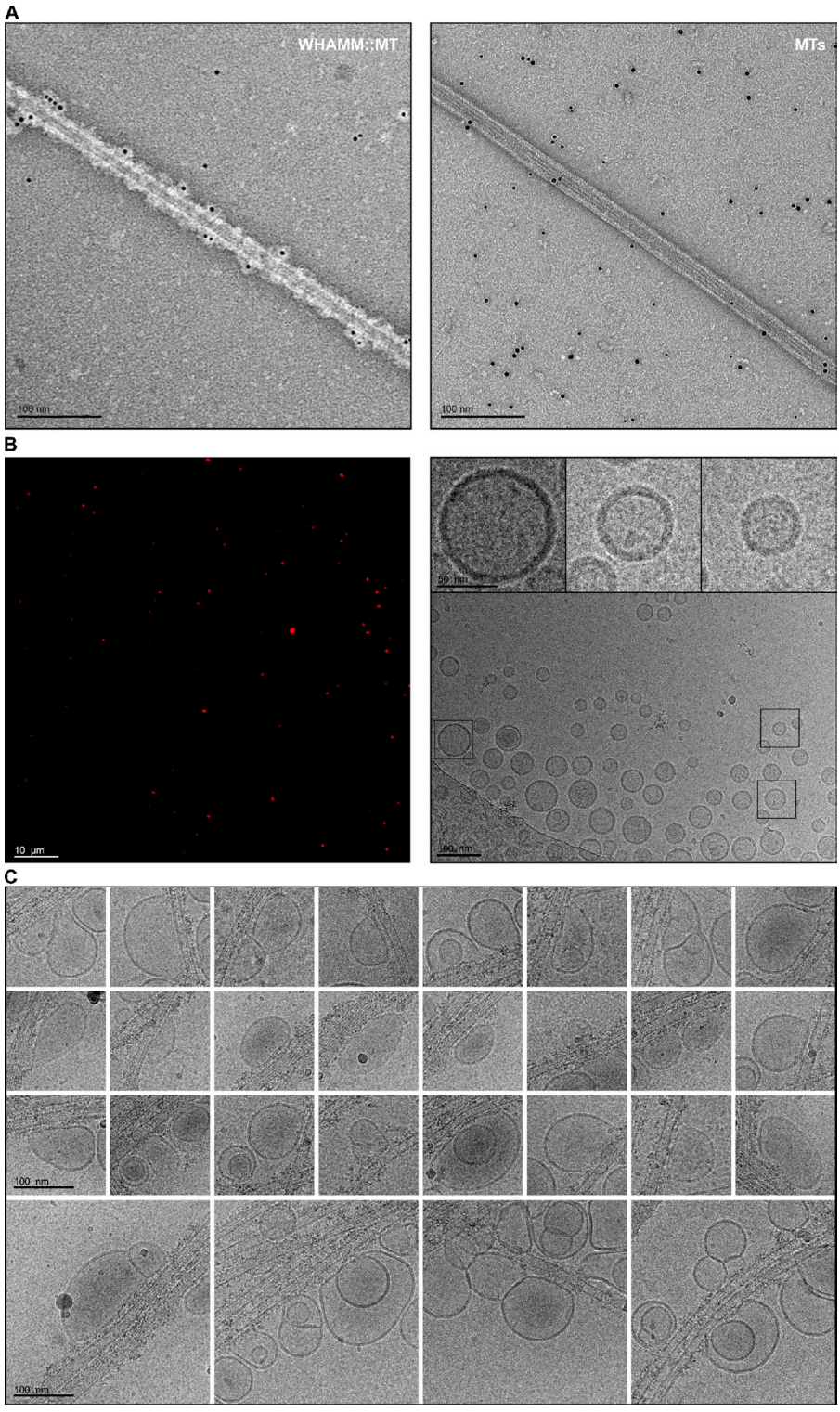

Figure S5. **The accessibility of the N-terminal His-tag of WHAMM when bound to MTs and the galleries of normal spherical liposomes and deformed liposomes bound to WHAMM::MT complexes.** (A) Ni-NTA–conjugated gold particles incubated with WHAMM::MT or naked MT. Representative EM pictures of gold particles binding to WHAMM::MT and not binding to MT are shown. (B) Typical fluorescence and cryo-EM images of normal spherical liposomes. The boxes were used to show the original selected liposomes in the image. And the insets are zoomed out images of these liposomes. (C) A gallery of deformed liposomes bound to WHAMM::MT complexes.

A supplemental file is also provided that contains the Matlab script for calculating the difference map between two 3D reconstructions.